WIND ENERGY
Wind Energ. (2008)
Published online in Wiley Interscience
(www.interscience.wiley.com) DOI: 10.1002/we.283

Research Article

Offshore Wind Profiling Using Light Detection and Ranging Measurements

Alfredo Peña*, Wind Energy Department, Risø National Laboratory for Sustainable Energy, Technical University of Denmark, Frederiksborgvej 399, 4000 Roskilde, Denmark and Department of Geography and Geology, University of Copenhagen, Øster Voldgade 10, 1350 Copenhagen, Denmark
Charlotte Bay Hasager, Sven-Erik Gryning, Michael Courtney, Ioannis Antoniou and Torben Mikkelsen, Wind Energy Department, Risø National Laboratory for Sustainable Energy, Technical University of Denmark, Frederiksborgvej 399, 4000 Roskilde, Denmark

Key words:
LiDAR; offshore; surface layer; wake; wind profiles

世界最大の洋上ファーム
Horns Rev(Vestas V80 × 80基)での6ヶ月間観測

The advantages and limitations of the ZephIR®, a continuous-wave, focused light detection and ranging (LiDAR) wind profiler, to observe offshore winds and turbulence characteristics were tested during a 6 month campaign at the transformer/platform of Horns Rev, the world's largest wind farm. The LiDAR system is a ground-based sensing technique which avoids the use of high and costly meteorological masts. Three different inflow conditions were selected to perform LiDAR wind profiling. Comparisons of LiDAR mean wind speeds against cup anemometers from different masts showed high correlations for the open sea sectors and good agreement with their longitudinal turbulence characteristics. Cup anemometer mean wind speed profiles were extended with LiDAR profiles up to 161 m on each inflow sector. The extension resulted in a good profile match for the three surrounding masts. These extended profiles, averaged over all observed stabilities and surface roughness lengths, were compared to the logarithmic profile. The observed deviations were relatively small. Offshore wind farm wakes were also observed from LiDAR measurements where the wind speed deficits were detected at all LiDAR heights. Profile-derived friction velocities and roughness lengths were compared to Charnock's sea roughness model. These average values were found to be close to the model, although the scatter of the individual estimations of sea roughness length was large. Copyright © 2008 John Wiley & Sons, Ltd.

Received 17 March 2007; Revised 26 May 2008; Accepted 8 June 2008

Introduction

Vertical wind speed profiles have mainly been measured on land and the results are commonly fitted into the surface layer (~10% of the atmospheric boundary layer) with a wind profile based on surface layer theory and Monin–Obukhov scaling.[1] For horizontally homogeneous and stationary flow, this corresponds to

$$\bar{u} = \frac{u_*}{\kappa}\left[\ln\left(\frac{z}{z_o}\right) - \psi_M\left(\frac{z}{L}\right)\right] \quad (1)$$

* Correspondence to: Alfredo Peña, Wind Energy Department, Risø National Laboratory for Sustainable Energy, Technical University of Denmark, Frederiksborgvej 399, 4000 Roskilde, Denmark.
E-mail: alfredo.pena.diaz@risoe.dk

where $\bar{u}$ is the mean wind speed at height z; u_* is the friction velocity; κ is the von Karman constant (~0.4); z_o is the aerodynamic roughness length, and ψ_M is the universal stability function. This last term depends on both the height and the Obukhov length L.

For wind resource assessments, equation (1) has been used to extrapolate wind speed measurements normally performed at low heights, e.g. 10 m. The vertical wind profile is determined from equation (1) by estimating u_* and L, e.g. from measurements of turbulence fluxes. The surface roughness length z_o can be estimated in relation to the land cover or by using roughness models for the sea state.[2] Equation (1) has been validated from experiments at heights up to 32 m (e.g. the Kansas experiment[3]) and 50–80 m in Gryning *et al*.[4] Beyond these levels, deviations have been reported in different boundary layer studies. The height of the boundary layer is introduced in Gryning *et al*.[4] as a length scale to correct vertical wind profiles measured up to 250 m. The inversion height is estimated in Lange *et al*.[5] from air density differences to correct offshore wind profiles at Rødsand (Denmark). These attempts to extend vertical profiles are important for the development of the wind energy because the knowledge of the wind resource at high levels in the atmosphere is still immature.

Conventional techniques (e.g. cup and sonic anemometers) have been extensively used to observe winds and turbulence. They have reached a limit in the vertical range which is similar to the current turbine's hub height. This is due mainly to the costs of erection of such high masts. At offshore locations, the situation is more complicated because the environmental conditions are harsher and the structural problems greater. However, offshore siting is attractive to the wind industry due to high wind speeds and lower turbulence levels.

Light detection and ranging (LiDAR) technology is part of the so-called ground-based remote sensing techniques which have been improved to work with high accuracy. Previous campaigns have found a high correlation when ZephIR LiDAR observations were compared against cup anemometers for 10 min mean wind speeds. Linear regressions were made in Smith *et al*.[6] at different heights resulting in correlation coefficients around 0.98 with slopes close to unity and offsets lower than 0.15 ms^{-1}. The measurements were done over flat and homogeneous terrain, but the same LiDAR technology has started to be utilized in other environments like forests[7] and offshore.[8]

The campaign at Horns Rev represents one of the first wind assessments where the usefulness of this LiDAR unit for measuring offshore wind speed profiles has been tested. Three different offshore inflow wind conditions are studied: land-influenced wind, open sea wind (directly from the open sea) and wake from the wind farm. A similar study was made by Antoniou *et al*.[8] in the Nysted wind farm located in the Baltic Sea close to Rødsand (Denmark). A QinetiQ LiDAR prototype was operated there successfully on the farm's platform during a 2 month campaign under free and wake conditions. Direct comparisons with mast data were difficult due to the configuration of the wind farm. The mean wind speed LiDAR profiles were extended from mast profiles showing good agreement. Another ZephIR LiDAR evaluation was performed by Kindler *et al*.[9] at the Fino-1 platform in the German North Sea. The slopes of linear regressions between LiDAR and different cup anemometers at a 100 m high mast were around 0.99 with correlation coefficients near unity.

This article presents the first set of results concerning the ZephIR LiDAR evaluation at the Horns Rev wind farm. The description of the campaign and the wind farm, the inflow conditions, the meteorological masts and the LiDAR unit are presented in Description of the Campaign. Comparison of LiDAR and Mast Data shows LiDAR's ability to measure wind speeds and turbulence characteristics by direct comparison with the cup anemometers. The extension of the side-mounted cup anemometer profiles to higher levels with LiDAR measurements is done in Extension of Wind Profiles Using LiDAR Data followed by a comparison with equation (1) assuming neutral conditions. Profile-derived sea surface roughness lengths and friction velocities are estimated from the model. These profile-derived averages are compared to Charnock's sea roughness model. Conclusions are drawn in the final section.

Description of the Campaign

The Wind Farm

The Horns Rev offshore wind farm is located in the North Sea at the West Coast of Jutland (Denmark) at approximately 30 km West of Esbjerg (see Figure 1).

DOI: 10.1002/we

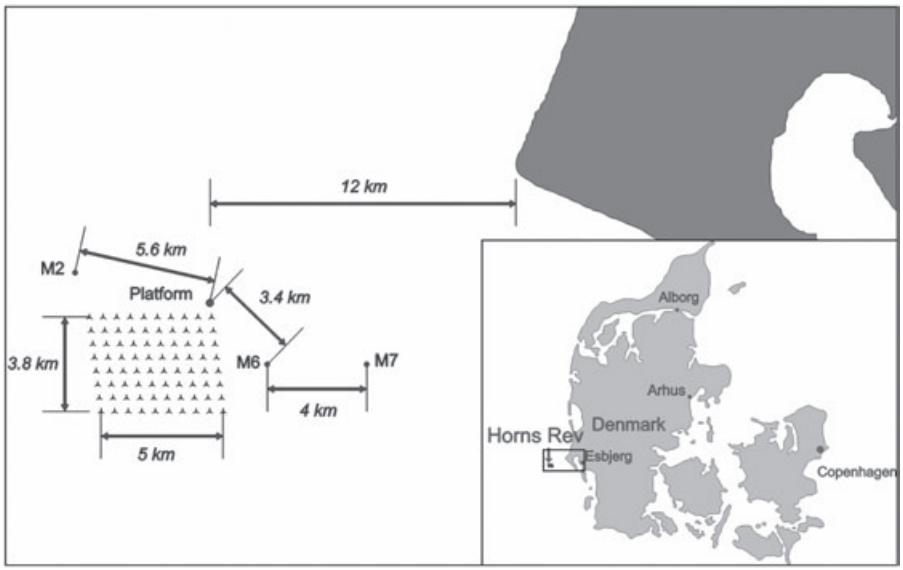

Figure 1. Horns Rev wind farm

Table I. Geographical coordinates of the masts and the platform at Horns Rev

Station	Latitude	Longitude	Distance/direction from closest turbine
M2	55°31′08.81″	7°47′15.07″	2 km north
M6	55°29′12.54″	7°54′43.56″	2 km east
M7	55°29′14.16″	7°58′31.20″	6 km east
Platform	55°30′31.03″	7°52′27.76″	0.5 km north

The farm consists of 80 Vestas V80 turbines with hub heights at 70 m above mean sea level (AMSL) and rotor diameters of 80 m; thus, the blade tip reaches 110 m height. They were installed in an oblique rectangle of 5 × 3.8 km formed by 8 horizontal and 10 vertical rows. Three meteorological masts were installed near the farm: Masts 2 (M2), 6 (M6) and 7 (M7) (The coordinates are given in Table I). M2 was installed for the evaluation of the resource during the wind farm planning. M6 and M7, respectively, are twin masts which are observing the wind farm wake from the dominant westerly sectors.

Inflow Wind Conditions

Three different inflow conditions are clearly observed at all locations where the platform and the meteorological masts are installed (see also Figure 2 and Table II):

1. 'Land-influenced': wind coming from the easterly sectors. This is directly influenced by the land (where Jutland is located).
2. 'Open sea': wind coming from the northwesterly sectors (directly from the open sea).
3. 'Wake': wind influenced by the farm wake. The direction range depends on the mast/platform position.

These conditions were selected due to the characteristics of the inflow wind. For easterly winds, a clear diurnal temperature cycle can be observed, indicating that the land influence is still significant. This is not the case for the westerly sectors as illustrated in Figure 3.

The coast line is approximately 20 km east from M2. Due to the generally lower turbulent levels, the effects of inhomogeneities (e.g. wind farms, structures, islands) are more pronounced than would be seen over land.

DOI: 10.1002/we

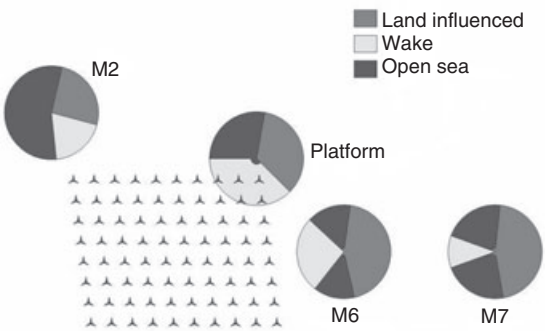

Figure 2. Inflow sectors at each location on Horns Rev

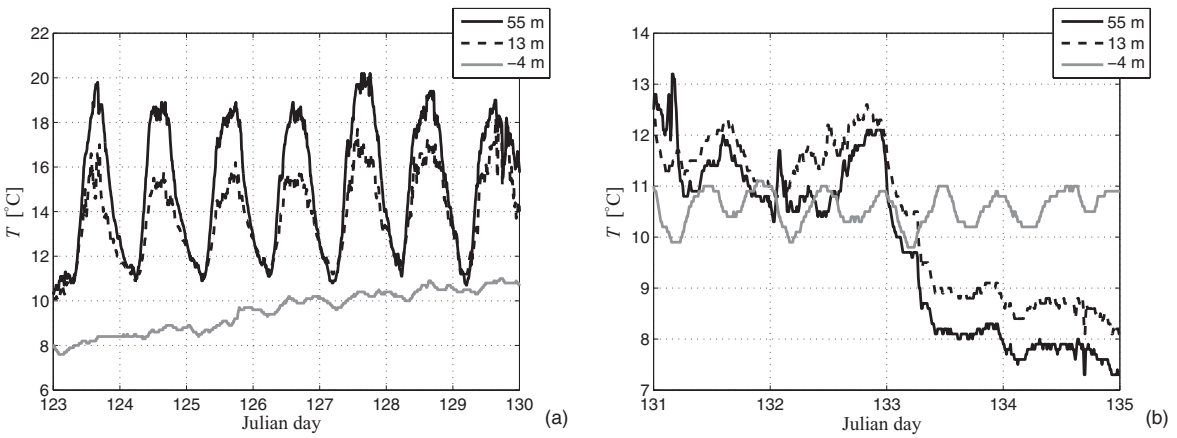

Figure 3. Air and water temperatures at M2 for (a) easterly winds (50–150°) and (b) westerly winds (210–360°)

Table II. Direction range of each inflow sector at all locations on Horns Rev

Location	Open sea (degree)	Land influenced (degree)	Wake (degree)
M2	174–13	13–105	105–174
Platform	270–10	10–135	135–270
M6	313–8 and 167–218	8–167	218–313
M7	285–6 and 170–250	6–170	250–285

The north corresponds to 0°. The direction is clockwise.

Wake effects were analysed in Christiansen and Hasager[10] where wind speed deficits were observed at 20 km distance from the wind farm using satellite measurements under near-neutral conditions.

Meteorological Masts

Data from the three surrounding masts were used for the study. These have lattice structures with square cross sections. The length of the cross section varies linearly from about 2.5 m at 20 m AMSL to 1.3 m at 60 m AMSL. Cup anemometers are mounted on booms that intersect the cross section diagonally and extend 2 m from the mast corners (see Figure 4(a)). An additional cup anemometer is mounted on a 2 m central pole at the top of the masts.[11] The data logging system collected meteorological observations at 2 Hz. The data were stored as 10 min mean averages. The instrumentation of each mast is given in Table III.

DOI: 10.1002/we

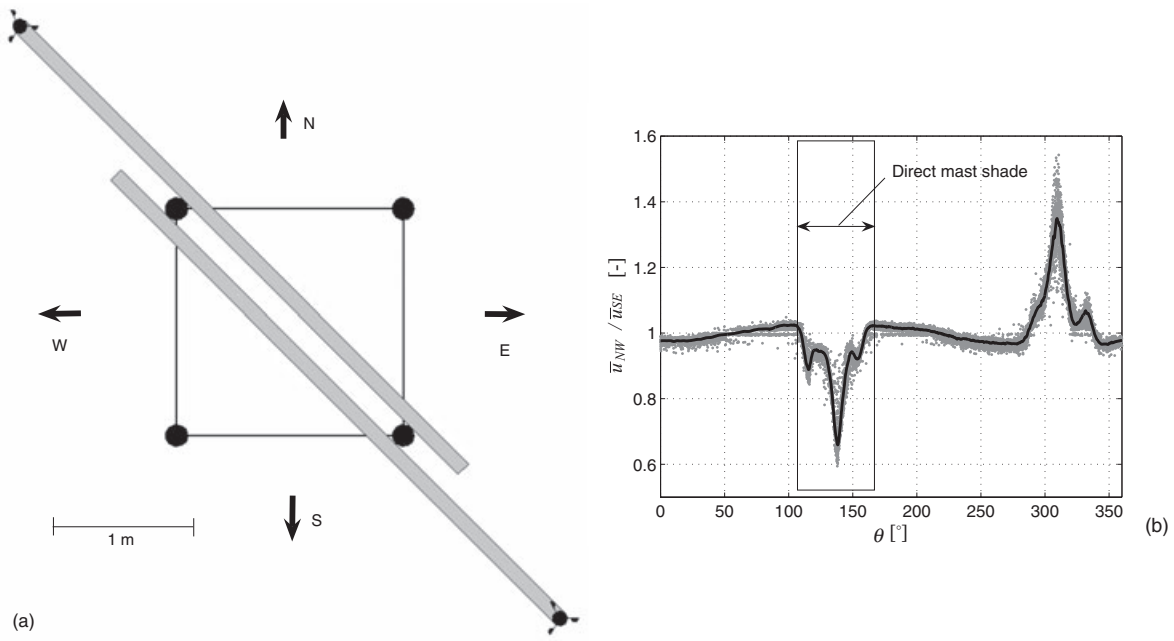

Figure 4. (a) Schematic of the M6 mast cross section showing the diagonally mounted booms. The booms are mounted from southwest to northeast at M2 (not shown). (b) Relative cup anemometer wind speed on M6 at 30 m AMSL on all wind directions θ. The excluded range is shown for the northwest cup anemometer

Table III. Mast instrumentation at Horns Rev

Mast	Height AMSL (m)	Instrument	Position on boom
M2	62	One cup anemometer (ms^{-1})	Top
	45	Two cup anemometers (ms^{-1})	SW and NE
	30	Two cup anemometers (ms^{-1})	SW and NE
	15	Two cup anemometers (ms^{-1})	SW and NE
	60	Wind vane (degree)	SW
	43	Wind vane (degree)	SW
	28	Wind vane (degree)	NE
	55	Temperature sensor (ºC)	NE
	13	Temperature sensor (ºC)	NE
	–4	Temperature sensor (ºC)	Sea
	13	Air relative humidity sensor (%)	NE
	55	Air pressure sensor (hPa)	NE
	13	Irradiation sensor (Wm^{-2})	SW
	13	Rain detector (mm)	SW
M6 and M7	70	One cup anemometer (ms^{-1})	Top
	60	One cup anemometer (ms^{-1})	NW
	50	Two cup anemometers (ms^{-1})	NW and SE
	40	One cup anemometer (ms^{-1})	NW
	30	Two cup anemometers (ms^{-1})	NW and SE
	20	One cup anemometer (ms^{-1})	NW
	68	Wind vane (degree)	NW
	28	Wind vane (degree)	NW
	64	Temperature sensor (ºC)	SE
	16	Temperature sensor (ºC)	SE
	–4	Temperature sensor (ºC)	Sea
	16	Air pressure sensor (hPa)	SE

The masts are operated by DONG Energy.
NE = northeast; SW = southwest; NW = northwest; SE = southeast.

DOI: 10.1002/we

The observations were selected at the southwest cup anemometers on M2 and northwest cup anemometers on M6 and M7. This is due to cup anemometer malfunctioning at 15 m northeast on M2 and at 20 m on M6 during the campaign period. All observed heights were guaranteed to have the same amount of data.

Five different types of uncertainties could be envisaged from the observations at the cup anemometers:

1. Direct flow distortion by mast shade. This can be extracted by plotting the cup anemometer speed ratio at each height where two cup anemometers are available. Measurements from these sectors are rejected for the analysis (see Figure 4(b)).
2. Non-direct flow distortion. The mast, booms and other parts of the structure influence the cup anemometer measurement beyond the mast shade on Figure 4(b). An analysis of the maximum wind speed deficits which can be found on each inflow wind sector is performed in the Appendix. Although the model accounts for the geometrical properties of the mast, the cup anemometer observations were not corrected as the model assumes flow conditions which could increase the error in the measurements (see Mean Wind Speeds). Nevertheless, it gives a good indication of the measurement uncertainty.
3. Cup anemometer overspeeding. The measurements are performed using Risø cup anemometers. This effect has a low influence on the observations according to Pedersen[12] and is neglected for the study.
4. Speed-up effects. The observations at the top-mounted cup anemometers can be influenced by flow speed up due to the proximity to the mast structure. They are mounted on 2 m long poles to avoid this effect. Nevertheless, the ratio between half the length of the top mast cross section and the pole length is small (~1.0 : 3.4) for all masts. A value around 1 : 5 would be advisable according to 61400-12-1 IEC.[13]
5. Calibration. The typical uncertainty in the wind speed measurement performed by a Risø cup anemometer is around ±1%. Cup anemometers are exchanged to freshly calibrated instruments about every 6 months.

The LiDAR Instrument

For the campaign at Horns Rev, we used QinetiQ's ZephIR wind LiDAR. This consists of a continuous-wave laser operating at the eye-safe wavelength of 1.5 μm, with height discrimination achieved by focusing sequentially at a number of pre-programmed heights. By passing the focused laser beam through a continuously rotating prism, the beam forms a cone at $\phi = 30.6°$ to the zenith. In any given azimuth direction, LiDAR measures the line of sight or radial velocity, V_{LOS}, which contains resolved components of the horizontal and vertical wind speeds according to the equation

$$V_{\mathrm{LOS}} = abs|u\cos(\theta-\theta_{\mathrm{d}})\sin(\phi)+w\cos(\phi)| \tag{2}$$

where u and w are the horizontal and vertical wind speeds, respectively; θ is the instantaneous azimuth angle, and θ_{d} is the wind direction (see Figure 5(a)). Under the assumption that the flow is uniform throughout the entire measuring volume, the three unknowns in equation (2), u, w and θ_{d}, can be obtained using a non-linear least squares method applied to the measured data (θ, V_{LOS}).

Backscattered, Doppler-shifted light from the focus volume is mixed with the baseband light and the power of the resulting beating is measured in the LiDAR's photo detector. The analogue signal is sampled at 100 MHz and converted at 200 kHz to power spectra using a 256-point (time domain) FFT (Fast Fourier Transform). In order to obtain an acceptable signal-to-noise ratio, even in reasonably clean air, 4000 of these spectra are ensemble averaged to provide one Doppler spectra every 20 ms, corresponding to 7.2° of azimuth. From each of these spectra, the frequency of the peak value is obtained by calculating the centroid. This frequency corresponds linearly to the line-of-sight velocity for this azimuth.

In the current configuration, the ZephIR measures over three complete rotations of the prism at each of the programmed heights, taking exactly 3 s and providing 150 line-of-sight velocity measurements. When represented in a polar plot, the measurements ideally form a figure of eight (an example of the measurements is illustrated in Figure 6).

As implied in equation (2), the sign of the Doppler shift (and hence the sign of the line-of-sight velocity) is lost in the signal processing. This happens because the backscattered light is mixed with the baseband (the

DOI: 10.1002/we

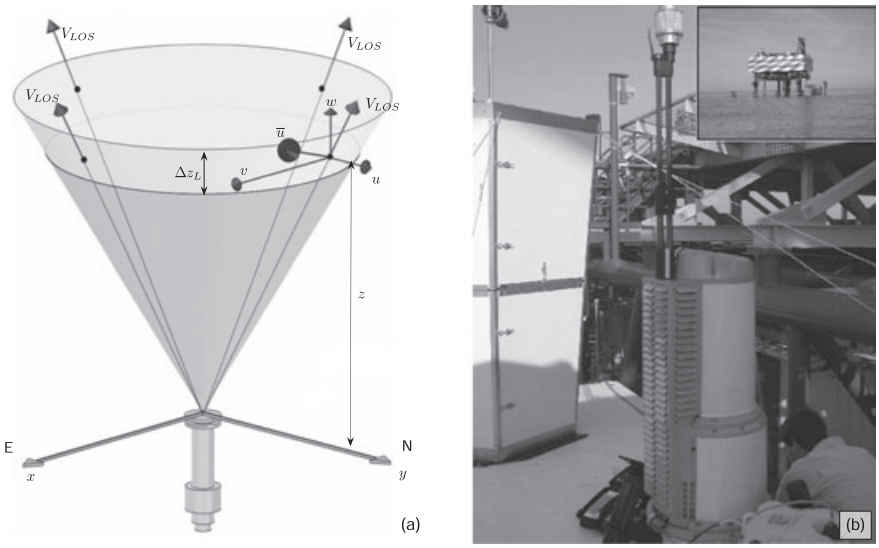

Figure 5. ZephIR wind LiDAR. (a) Scanning configuration. (b) Installation on the platform

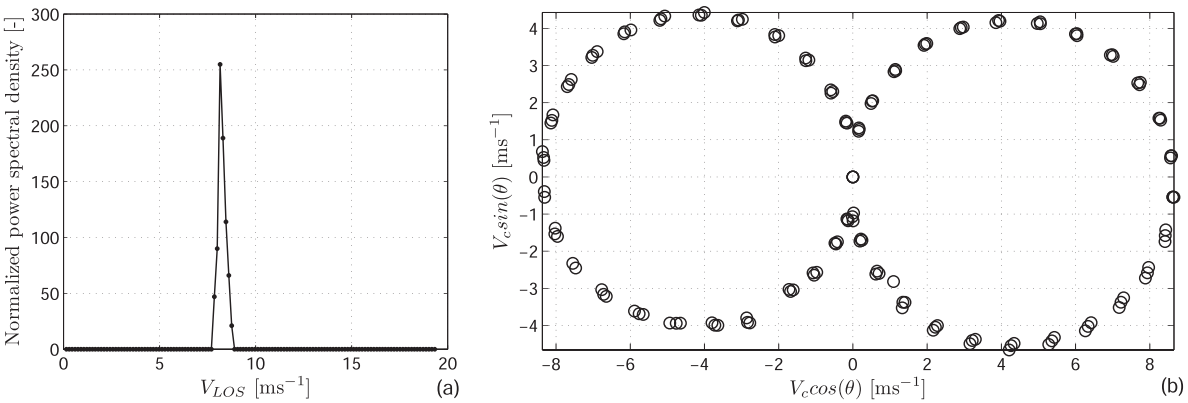

Figure 6. (a) Averaged Doppler-shifted spectrum at one single scan at 121 m height. (b) Figure of eight showing the measurements at 121 m during the 3 s period. V_c *corresponds to the centroid velocity value of each averaged Doppler-shifted spectrum*

laser source) frequency itself, without an offset being applied. In this case, a frequency shift of $+\delta_f$ and $-\delta_f$ give precisely the same beating pattern and cannot be distinguished from each other. Because of the rectification of the line-of-sight velocity, there are actually two possible solutions to equation (2). The signs of the direction and the vertical speed (although not their internal relationship) are ambiguous. We know the axis of the wind direction, but not from which side it blows. For this reason, the ZephIR is equipped with a thermal wind sensor mounted at the top of a small mast. Of the two wind directions possible from the fitted data, the one closest to the value from the wind sensor is chosen. If it is necessary to change the sign of the wind direction, then the sign of the vertical velocity must also be swapped in order to maintain the correct internal relationship.

Two levels of data are stored by the ZephIR on a removable flash disk. The speeds and direction obtained from each of the 3 s data, representing one height, are stored together with a so-called 'turbulence parameter'. This latter is in fact, a measure of the 'goodness of fit' and as such is influenced mainly by turbulent fluctuations (within the 3 s measuring period), but also by noise and other error conditions such as cloud effects (see

DOI: 10.1002/we

below). The 50 Hz Doppler spectra are also saved on the flash disk, consuming a vast majority of the available storage.

Ten minute mean values and standard deviations can also be extracted from the ZephIR but are calculated 'on the fly' from the stored 3 s data. It should be noted that one measurement at one height takes 3 s. The focus is then moved to the next height and a new 3 s period begins. Including the time for refocusing, a complete cycle of five heights takes about 18 s. In one 10 min period, at each height, there will be around 26 samples, each scanned over a period of 3 s and with a gap of about 15 s.

Measurement Imperfections

Inherent in the design of a focused LiDAR system is that the vertical measuring length (the probe length Δz_L in Figure 5(a)) increases with the square of the measuring height. For the optics of the ZephIR, the probe length is about 20 m at 100 m measuring height. Above 150 m, the probe length becomes unacceptably large, and this represents the upper limit of measuring height for this design. Within the measuring volume, the intensity of the focused beam and, assuming a constant aerosol profile, the backscatter intensity are weighted vertically by a Lorentzian function with a maximum at the focus point. Linear profiles will weight symmetrically about the focus point and in theory, LiDAR will report exactly the same mean speed as from a point measurement at the focus point, despite the finite probe length. This is not the case for non-linear profiles, and this can introduce a small error. For a logarithmic profile, the error is typically about 0.15% at 100 m.

An extreme case of aerosol non-uniformity that we are obliged to consider is when low clouds are present. The backscatter coefficient from the water droplets at the base of the cloud is several orders of magnitude higher than from the background aerosol. Even though the cloud base (say at 1500 m) is way outside the focal range, the cloud backscatter, Doppler shifted at the speed of the cloud, is so intense that it can be of comparable or larger magnitude than the focused backscatter from the nominal measuring height when measured at the photodetector. Unless corrected for, this spurious spectral content will normally result in an overestimation of the wind speed (since clouds are higher and therefore usually faster).

The ZephIR has a cloud-correction algorithm based on an attempt to measure and correct for the spectral content from the clouds, by focusing at an extra, higher height, usually 300 m. This spectral content is then simply subtracted from the spectra measured for the lower heights (on a per azimuth basis). The internal cloud-correction algorithm was not used for the Horns Rev measurements. Instead, we attempted to identify periods with low clouds from the ratio of the backscatter at the different heights. The idea here is that with no cloud present, the backscatter from all heights will be approximately equal (a general characteristic of a focused LiDAR system). When clouds are present at the higher focus heights, they have a significantly higher backscatter than lower heights. Such periods are filtered from the final data using the spectra scaling factor which is inversely proportional to the backscatter. Data with a scaling ratio above 1 (between the lowest and the highest observation heights) were rejected for the study (see Figure 7). This corresponds to approximately 20% of the whole Horns Rev data set.

Experimental Setup

The LiDAR was installed on the platform at 20 m AMSL. Initially, measuring heights (AMSL) of 46, 63, 91 and 121 m were chosen. From visual inspection of the LiDAR data, significant non-zero vertical velocities could be seen for the lowest height, indicative of flow distortion due to the platform structure. It was therefore decided to abandon the lowest measuring height and instead increase the upper limit of the profile by 40 m. We thus ended with the measuring heights of 63, 91, 121 and 161 m AMSL. A fifth LiDAR measuring height of 320 m AMSL was used to provide spectral data pertaining to cloud presence.

The ZephIR measures autonomously and stores processed data on a 4 GB compact flash card. Data can be accessed either remotely using a GSM (mobile telephone), locally over a network connection or by physically removing the flash card and copying the data directly to a computer. Remote access with GSM is so slow that it can only be used for checking system operation and retrieving 10 min mean values of the measured data. Physical access to LiDAR was impractical and very costly at the offshore platform. In order to save data at

DOI: 10.1002/we

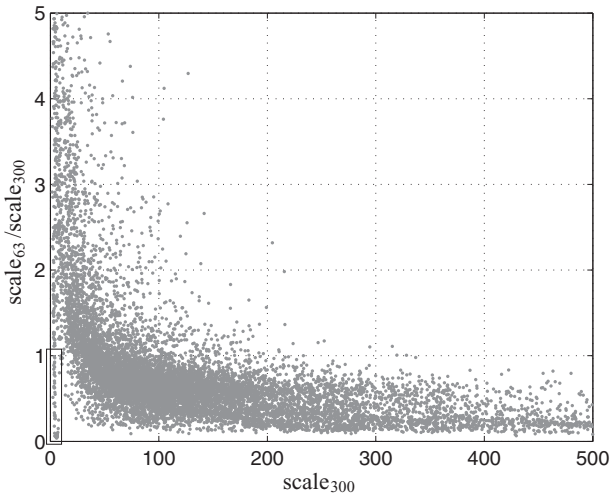

Figure 7. Spectra scaling factor ratio between the lowest and highest height. The x*-axis represents the absolute value of the backscatter at 300 m and decreases to the right. Data on the left corner box were also rejected due to possible contamination of the spectra with fog or low clouds*

Table IV. Data availability during the campaign

Instrument	Availability (%)
M2	99.32
M6	91.09
M7	91.01
LiDAR	44.85

Percentages correspond to non-filtered data.

the lowest level of processing (the 50 Hz Doppler spectra) and at the same time, to avoid frequent trips to the platform, a PC was dedicated to receive spectra streamed from the LiDAR. This PC was placed on the wind farm's network, giving access to the Internet for outgoing data and permitting remote control via a virtual private network. Initially, this PC was placed at the land end of the wind farm network in Esbjerg. The LiDAR and the PC communicated directly over the network. It became quickly apparent that the communication protocol between the LiDAR and the PC required a very low level of extraneous traffic on the network. This could not be accomplished with the two systems physically separated, and as a consequence, the PC was moved out to the platform with a private network connection to the LiDAR. Spectra were streamed to the PC using a modified version of the host program supplied with the ZephIR. The data were saved as hourly files, stored on the local hard disk and also transmitted to Risø using a standard FTP protocol.

After relocating the PC out to the offshore platform, close to the LiDAR, the system reliability improved considerably. However, the QinetiQ software was a relatively early version and was not completely stable. The streaming would stop irregularly with a mean interval of about 3–5 days. Using the remote control connection from Risø, we were always able to restart the software, but this problem caused a significant fall in data availability.

A more serious problem occurred on 8 June 2006. Contact to LiDAR was lost and could not be reestablished. No further data were recorded until 27 August 2006, following a trip to the offshore platform. The failure was caused by salt water leaking into the (external) LiDAR power supply. An improvement to the waterproofing of the power supply box was improvised and the problem did not recur.

The campaign with LiDAR started on 3 May and ended on 24 October 2006. The availability of the data for the masts and LiDAR is shown in Table IV.

DOI: 10.1002/we

Conversion of the raw Doppler spectra to fitted 3 s speeds and direction takes place using an algorithm that is very close to that used internally by LiDAR. The data used in this analysis are calculated using the Risø algorithm.

Comparison of LiDAR and Mast Data

LiDAR measurements were compared to cup anemometer data from the three masts for the open sea sectors at their overlapping heights (the 'land-influenced' sectors were excluded due to the variation in fetch distance).

Mean Wind Speeds

The correlation between 10 min mean wind speeds is shown in Figure 8.

All three resulting correlations and their respective regressions show high agreement. Given the large distance between the platform and masts and the high correlation observed, the open sea flow can be said to be highly homogeneous. The highest correlation is observed for M6, which is the mast closest to the platform. The slopes for M6 and M7 are close because they observe the same height. The observations for M2 are at

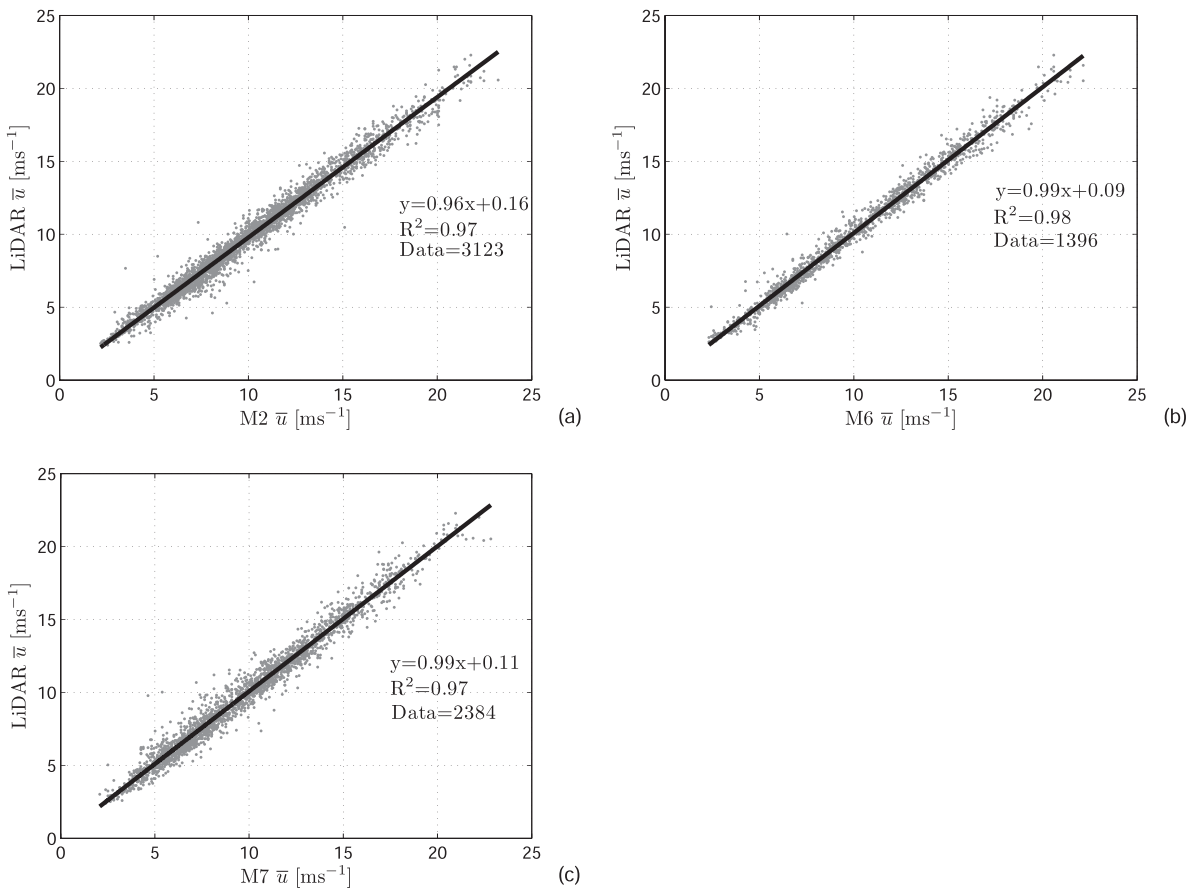

Figure 8. Comparison of horizontal wind speeds from LiDAR against cup anemometers. (a) LiDAR at 63 m and M2 at 62 m (top-mounted cup anemometer). (b) LiDAR at 63 m and M6 at 60 m (side-mounted cup anemometer). (c) LiDAR at 63 m and M7 at 60 m (side-mounted cup anemometer)

DOI: 10.1002/we

the same LiDAR height, but the slope gives the lowest value (the cup anemometer measures a higher wind speed).

The observations for M6 and M7 are from side-mounted cup anemometers. The low offsets in their regressions may be related with non-direct mast distortion. Nevertheless, these offsets are dependent on the selected wind speed range. The model in the Appendix indicates differences on the cup anemometer measurements relative to the wind direction but does not take into account the wind speed and the turbulence level. The complexity of these phenomena is the reason why the cup anemometer observations were not corrected for non-direct flow distortion. It is assumed that the effect is the same for the different cup anemometers on the same row of the mast. Rain data as well as wind speeds below 2 ms^{-1} were also rejected for the study.

Turbulence Observed by LiDAR

Turbulence measurements of the standard deviation of the longitudinal component of the wind speed σ_u from LiDAR were compared against turbulence measurements from the cup anemometers at the three masts. Figure 9 shows these comparisons of the standard deviation over a 10 min averaging period.* Although the agreement is generally good, the slopes of the linear regressions are less than unity and range from 0.73 (M2) to 0.82 (M6). Attenuation of the LiDAR-measured standard deviation relative to cup anemometer

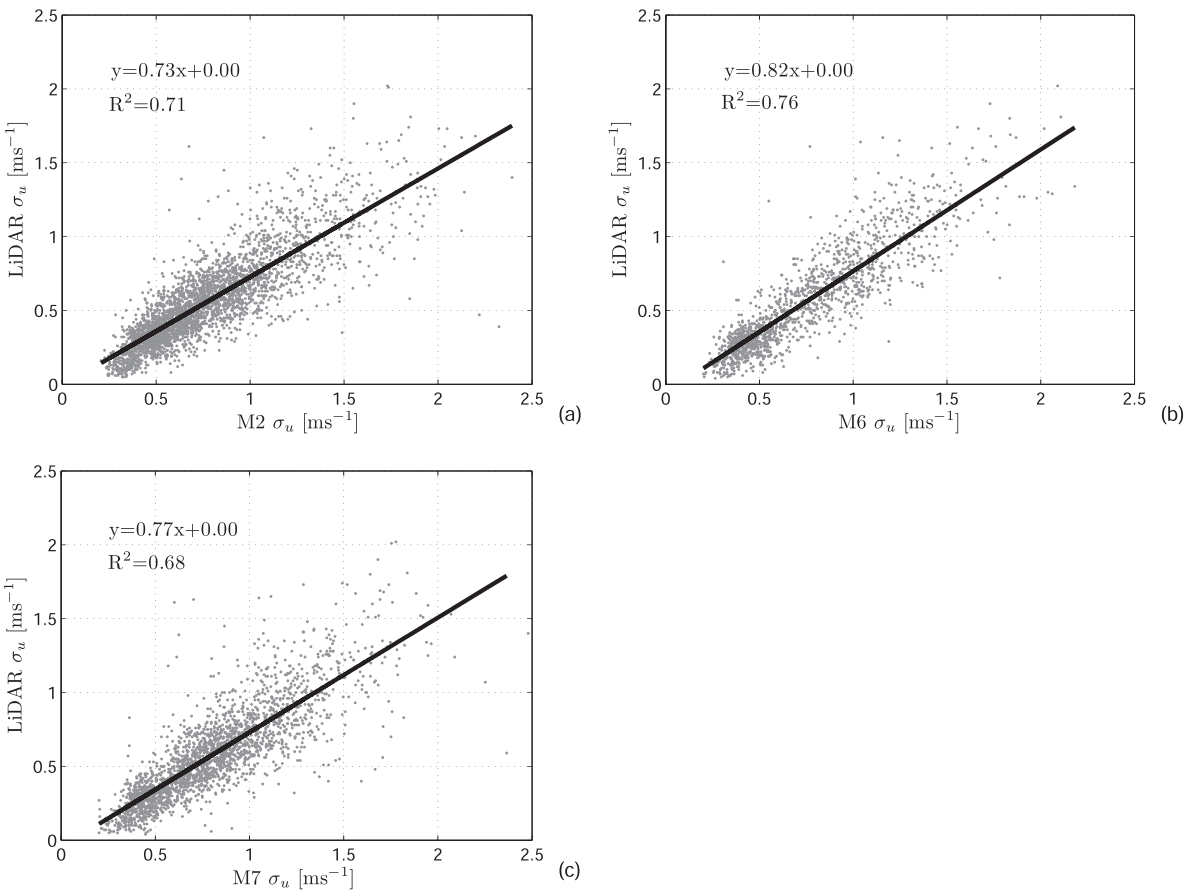

Figure 9. Comparison of σ_u from LiDAR against cup anemometer measurements. (a) LiDAR at 63 m and M2 at 62 m. (b) LiDAR at 63 m and M6 at 60 m. (c) LiDAR at 63 m and M7 at 60 m

*The comparisons made in this section have the same amount of data used for Mean Wind Speeds.

DOI: 10.1002/we

measurements has already been predicted,[14] and is a consequence of LiDAR's relative large effective measuring volume and its present 3 s three-revolution scanning configuration. Current campaigns using similar LiDAR units are observing the same behavior. These are taking place at the National Test Site for Wind Turbines in Høvsøre and at a forest in Sorø (Denmark).[7]

Turbulence is important for the performance of the wind turbine. The turbine's power production depends (among other factors) on the turbulence level.[15] The dynamic loading of the structure is dependent on the wind speed fluctuations. A measure of the turbulence level is given by the so-called turbulence intensity defined by

$$I_{\mathrm{u}} = \frac{\sigma_{\mathrm{u}}}{\overline{u}} \tag{3}$$

where I_{u} is the longitudinal turbulence intensity. This increases at low wind speeds over land due to atmospheric stability effects. The process is similar over the water, but the roughness length increases with wind speed. The turbulence intensity will increase at a certain wind speed due to the increasing roughness. In Figure 10, the turbulence intensity is compared from the LiDAR measurements (the horizontal component) and the corresponding observations from the cup anemometers at the different masts.

LiDAR measurements follow the behavior of the cup anemometer at all masts where the turbulence intensity decreases with wind speeds up to 10 ms^{-1}. Beyond this level, both LiDAR and cup anemometer turbulence intensities increase. The difference observed between the LiDAR and the mast curves is mainly due to the

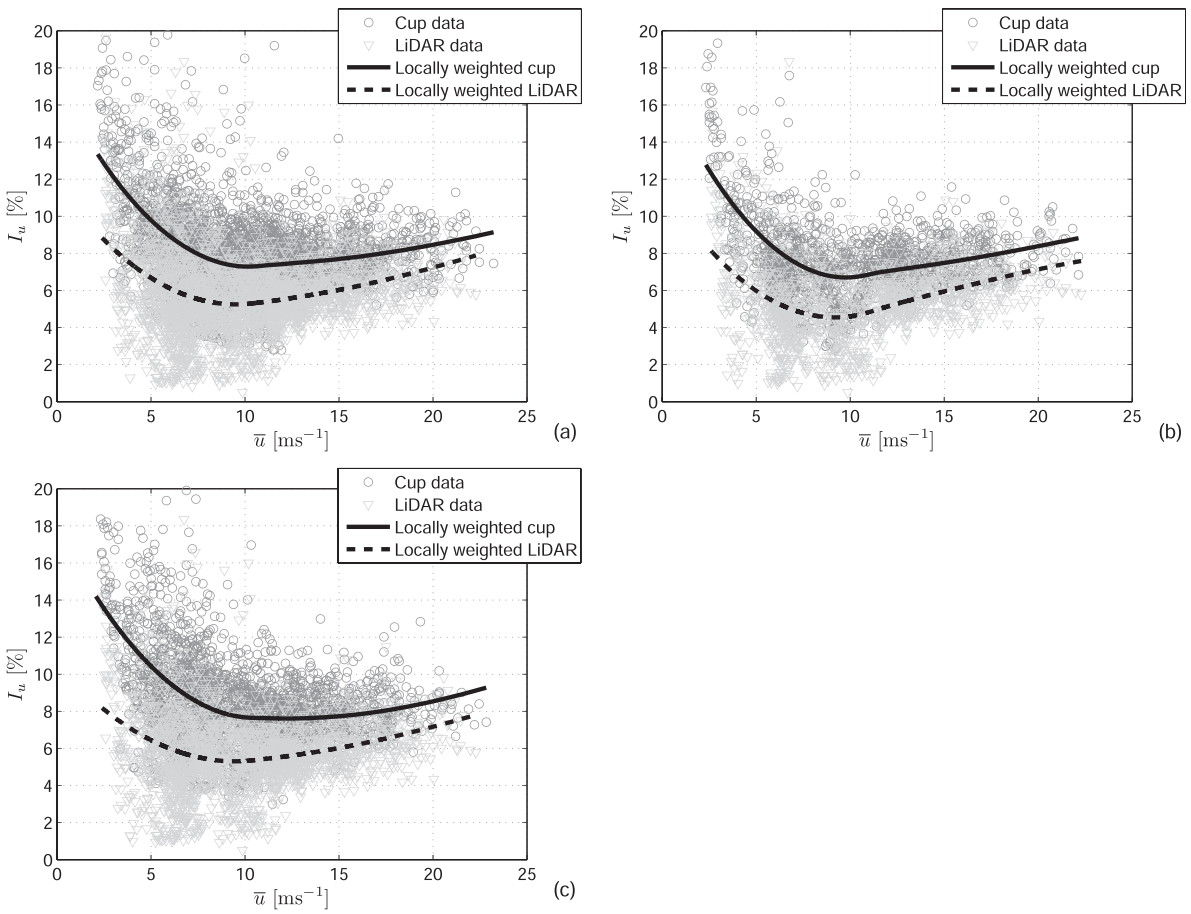

Figure 10. Comparison of turbulence intensities from LiDAR against cup anemometer measurements. The locally weighted curve smoothes the data using a least squares quadratic polynomial fitting. (a) LiDAR at 63 m and M2 at 62 m. (b) LiDAR at 63 m and M6 at 60 m. (c) LiDAR at 63 m and M7 at 60 m

DOI: 10.1002/we

attenuation of the standard deviation. Figure 10 indicates that the degree of attenuation is dependent on the wind speed. This can be also observed from Figure 9. The scatter on these graphs is concentrated below the regression line for low σ_u cup anemometer values (<=0.5 ms^{-1}). The ZephIR LiDAR underestimates turbulence for low wind speeds to a higher degree as it does for high wind speeds.

Extension of Wind Profiles Using LiDAR Data

Mean wind speed profiles are extended up to 161 m AMSL by combining the cup anemometer and LiDAR profiles. The extension is performed for the three different inflow conditions when the inflow sector on each mast overlaps the same sector observed on the platform (see Figure 11).

The amount of data at each height is the same for the whole extended profile. The number of measured 10 min wind speed profiles on each inflow sector is given in Table V.

LiDAR and cup anemometer profiles do not match on the 'wake' sector because the direction to the farm is different for each mast and platform location. Both match well on the open sea and land-influenced sectors at all mast locations. Standard errors at all heights are relatively small including the measurements from M2 on the land-influenced sector. This has the smallest number of measured profiles.

At Horns Rev, previous measurements, e.g. in Elsam Engineering[11] and Tambke *et al.*,[16] have shown a pronounced discontinuity in the wind speed profile at the top-mounted cup anemometer on M2 and M6. From

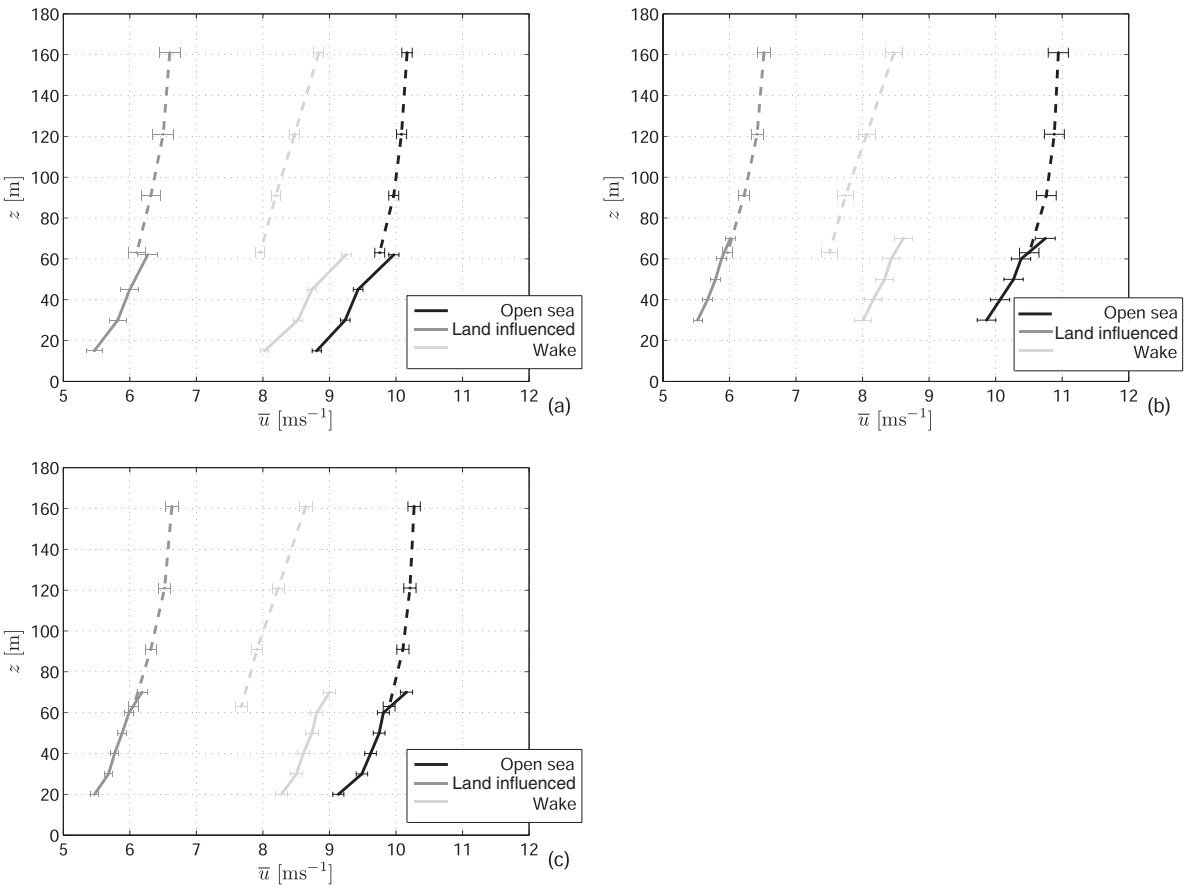

Figure 11. Extended mean wind speed profiles from cup anemometers with LiDAR measurements. The dashed lines correspond to LiDAR and the solid lines to cup anemometers. (a) Using M2. (b) Using M6. (c) Using M7. The ±1 standard error is indicated in the error bars

DOI: 10.1002/we

Table V. Number of measured profiles at the three different masts on each inflow sector

Location	Open sea	Land influenced	Wake
M2	2580	183	2177
M6	965	543	748
M7	1948	552	1450

Table VI. Maximum wind speed deficit/increment on each inflow sector

Location	Height (m)	Open sea	Land influenced	Wake
M2	45	0.98/1.02	1.02	0.98
	30	0.98/1.02	1.03	0.98
	15	0.97/1.03	1.03	0.97/1.01
M6 and M7	60	0.98	1.02	1.02
	50	0.98	1.02	1.02
	40	0.98	1.02	1.02
	30	0.98	1.03	1.03
M7	20	0.97	0.99/1.03	1.03

Figure 11, this occurs at all masts. The effect is observed in each sector and is relatively higher for the open sea than for the land-influenced inflow conditions. Observations below the top-mounted cup anemometer are not corrected for non-direct flow distortion, and the discontinuity may be partly due to a wind speed deficit on the side-mounted cup anemometers. Nevertheless, as given in Table VI, side-mounted cup anemometers may observe an increased wind speed for certain inflow conditions, in particular the whole land-influenced sector at M2 or wake sector at M6. The discontinuity can be observed even for these sectors in Figure 11. Here, a correction of the side-mounted cup anemometer observations would result in an even more pronounced discontinuity.

The deck of the Horns Rev platform is 23 m AMSL. Scaling of the model simulations by Bechmann[17] shows that above a bluff body of 20 m, the wind velocity deficit at 60 m above the surface varies between −0.5 and 1.0%. These computations were performed assuming a solid cube. At Horns Rev, these deficits are lower because the platform is standing on legs about 16 m AMSL (see Figure 5(b) at the top-right corner).

Comparison with Theoretical Profiles

The extended cup-LiDAR profiles are compared to the surface layer wind profile given in equation (1) by neglecting the stability dependence (i.e. $\psi_M \approx 0$). This gives the logarithmic profile expression

$$\overline{u} = \frac{u_*}{\kappa} \ln\left(\frac{z}{z_o}\right) \tag{4}$$

Equation (4) is assumed to be valid in the surface layer. u^* and z_o can be derived from the profile using measurements of mean wind speed at different levels:

$$\ln(z) = \frac{\kappa}{u_*}\overline{u} + \ln(z_o) \tag{5}$$

where u^* is proportional to the slope and z_o to the intercept $u = 0$. The calculation is made for all heights up to 45 m AMSL on M2 and 50 m AMSL on M6 and M7 where the surface layer is extended. The comparison

DOI: 10.1002/we

is shown in Figure 12. Measurements of the top-mounted cup anemometers are not included in Figure 12 because they do not follow the behavior of the side-mounted cup anemometer profiles (see Figure 11). It should be noted that the wind speed profile measurements in Figure 12 represent the mean over all observed stabilities and surface roughness lengths.

During the part of the year where the observations took place, the atmospheric stability over the sea was generally considered to be unstable. The deviations from the fitted profiles are small on all land-influenced and open sea inflow sectors. For the open sea sectors, the wind profile above the surface layer is seen to be near logarithmic or with a small overprediction of the measurements. Such wind profiles are typical for atmospheric unstable conditions.[4] On the land-influenced sectors at M6 and M7, the LiDAR measurements observe higher wind speeds because the fetch distance to the platform is larger than for both masts.

The wake reference profiles are taken from sectors where no wake is observed at each mast. Wind speed deficits from the wind farm wake are observed at all heights measured by LiDAR. In the most extreme case, i.e. where the highest wind speed deficit is observed at M7, the mean wind speed is reduced approximately 15% at hub height.

Sea Surface Roughness

The sea surface roughness depends on wind speed, fetch distance, atmospheric stability and water depth among other variables. In Comparison with Theoretical Profiles, profile-derived roughness lengths and friction veloc-

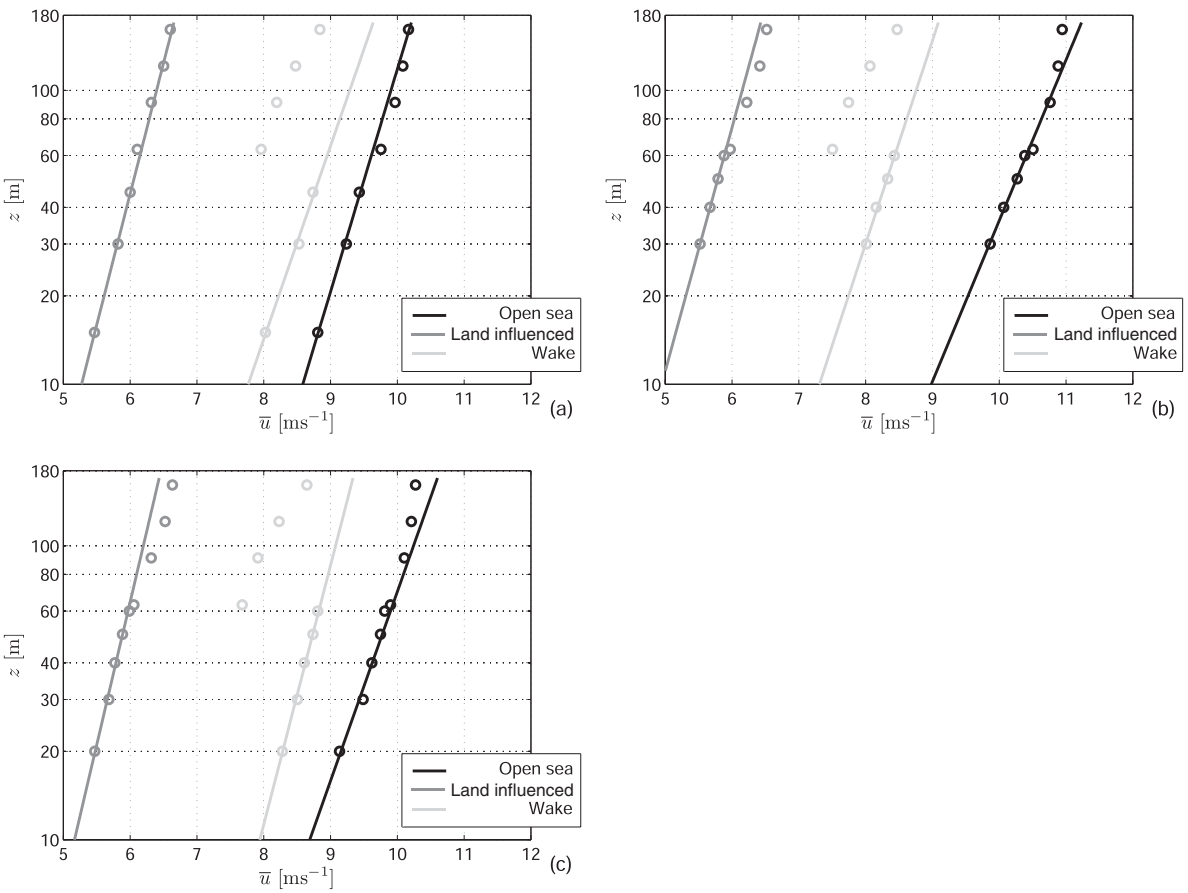

Figure 12. Comparison of measurements with mean wind speed profiles derived from the logarithmic profile (solid lines). (a) M2, (b) M6, (c) M7

DOI: 10.1002/we

ities were estimated assuming a logarithmic profile in the surface layer. They can be compared to Charnock's roughness model in Charnock[18] where the water waves are dependent on the friction velocity. This is given by

$$z_o = \alpha_c \frac{u_*^2}{g} \tag{6}$$

where α_c is Charnock's parameter (~0.012) and g is the gravitational acceleration. The comparison is shown in Figure 13. The scatter in the figure represents roughness length and friction velocity estimations (using a logarithmic profile fitting). They are found from individual 10 min wind speed profiles which are assumed to be close to neutral conditions. This neutral state is approached using the bulk formula for the drag coefficient given in Kraus.[19] This relates the heat flux $\overline{w'T'}$ with the drag coefficient C as

$$\overline{w'T'} = C_z \bar{u}_z (T_o - T_z) \tag{7}$$

where z is the reference height (at 15, 30 and 20 m AMSL for M2, M6 and M7, respectively), T_z the air temperature (the closest to the observed cup anemometer at each mast) and T_o the sea surface temperature (the sea temperature at –4 m is assumed to be close to the surface temperature). The smaller the absolute value of the term $\bar{u}_z(T_o - T_z)$, the smaller the heat flux.[†] This gives an indication of neutral stability.

Lower values of u^* and higher roughness lengths are observed for all masts on the land-influenced inflow sector due to the influence of the land roughness on the wind profile. The estimations on the land-influenced sector are always higher than the model which has been previously observed to work better for open sea than for coastal areas. The important observation is that although the scatter of all individual estimations of roughness length is large, the profile-derived mean values are near Charnock's model. The roughness length, in contrast with the friction velocity, is a highly sensitive parameter in equation (4). Thus, Charnock's relation is a useful tool to model sea roughness in the logarithmic profile.

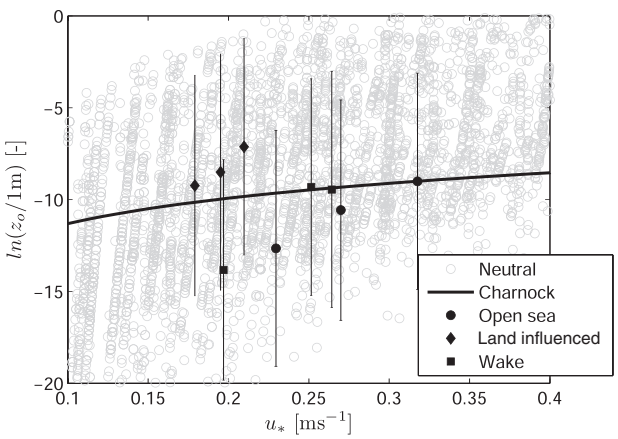

Figure 13. Comparison of estimated u_* *and* z_o *values with Charnock's sea surface model (solid line). The bars indicate the variability of the profile-derived roughness length when the estimation is done from the higher and lower values of wind speed at the error bar tails in Figure 11. The standard errors for the mean values of friction velocity are less than* $\pm 0.01\ ms^{-1}$

[†]The interval used is $|\bar{u}z(T_o - T_z)| \leq 2$. Assuming a drag coefficient of 1.2×10^{-3}, the absolute value of the heat flux is less than 2.4×10^{-3} Kms^{-1}.

DOI: 10.1002/we

Conclusions

The ZephIR LiDAR has been shown to be a potential useful tool for the evaluation of offshore wind resource once the system reliability is improved. In particular, this instrument has the ability to perform good wind profiling at heights up to 160 m AMSL where conventional techniques have reached limits in both the measurement range and their deployment conditions. The unit's accuracy has been tested by comparison against mean wind speeds between different masts.

The LiDAR observations of the standard deviation of the longitudinal wind speed component were found to be attenuated by the instrument relative to the cup anemometers due to LiDAR's effective measuring volume and its scanning configuration. Nevertheless, the turbulence intensity observed by LiDAR follows the turbulence intensity from the cup anemometers. LiDAR detects a variation of the turbulence intensity with wind speed.

Vertical wind profiles were extended from the cup anemometer profiles using LiDAR measurements, and the match was good at all mast locations and on the open sea and land-influenced sectors. The top-mounted and side-mounted cup anemometers at Horns Rev were observed to be differently influenced by the mast structure.

The logarithmic profile was found to agree closely with the extended cup-LiDAR profiles for the land-influenced and open sea sectors. Given that near-unstable atmospheric conditions are considered to prevail from the open sea sectors during this campaign, the measurements tend to agree with those of Gryning *et al*.,[4] which suggested a logarithmic profile during near-unstable conditions. The presence of land was observed from the differences found in the profiles observed at M6 and M7 on the open sea and land-influenced sectors.

Charnock's roughness length model was compared to wind profile-derived estimations of roughness length. Covering different stabilities and sea-state conditions, Charnock's relation was found in agreement with the estimated roughness lengths on all inflow sectors.

The wind farm wake could be detected up to 161 m AMSL from the LiDAR's measurements. The wake profile shows mean wind speed deficits between 10 and 15% at the wind turbine's hub height for all mast locations.

Future Work

Atmospheric stability plays an important role on the wind characteristics at Horns Rev. In this article, the profiles are averaged over different atmospheric conditions where the logarithmic profile fits the measurements well. Nevertheless, current analysis reveals great variations from the neutral state when the extended profiles are classified using a bulk formulation for the stability. These high profiles are being tested against standard models (e.g. the Businger–Dyer relations) and others which account for the influence of the height of the boundary layer. The state of the atmosphere may have an influence on the LiDAR observations as well as flow distortion effects on the masts.

Analysis of the wake of the wind farm using the LiDAR profiles is also envisioned. This is not simple due to the location of the platform with respect to the different rows of turbines in the wind farm. However, as it is shown in the article, wind speed deficits are detected comparing 'open sea' profiles observed at the masts.

Acknowledgements

The authors would like to thank Troels Friis Pedersen for the discussion about flow distortion around masts and its influence on cup anemometer measurements.

The LiDAR campaign was done by technical support from Risø's test and measurement division in cooperation with Paul B. Sørensen at DONG Energy. The campaign was funded by the Danish Research Agency, the Strategic Research Council, Program for Energy and Environment (Sagsnr. 2104-05-0013).

I also thank Professor Henrik Søgaard for PhD supervision.

DOI: 10.1002/we

Appendix

The analysis of the flow around a lattice structure is made in 61400-12-1 IEC.[13] Iso-speed plots are shown on Figure 14 for different positions of the boom relative to the wind direction θ_{rel}.

The values for the iso-speed curves are found by measuring the distance R of the extended circle at each boom position. The wind speed deficit u_d is estimated on the center line by

$$u_d = 1 - \left(0.062C_t^2 + 0.076C_t\right)\left(\frac{L}{R} - 0.082\right) \tag{8}$$

where L is the length of the mast cross section and C_t is the thrust coefficient. An estimation of the thrust coefficient is given by

$$C_t = 2.6(1-t)t \tag{9}$$

where t is the mast solidity. This is estimated at each height on the three masts from the geometry of the sections. Equation (8) can be used to plot the variation of wind speed deficits with relative wind direction. This is shown on Figure 15 for M2 and M6 at each height.

In Figure 15 are also shown the intervals where the inflow wind sectors are found. The maximum values of wind speed deficits on each sector are given in Table VI. These are in agreement with the findings made by Højstrup.[20]

The wind speed deficits are computed in Figure 15 until the cup anemometer is well inside the direct mast shade area, which gives a maximum relative wind direction of around 160º. Although the thrust coefficient is different for each mast section, the largest wind speed deficits are found in the lowest levels due mainly to the decrease in section area with height (proportional to the term L/R in equation (8)) where the cup anemometers are separated from the mast square section by the same distance at all heights.

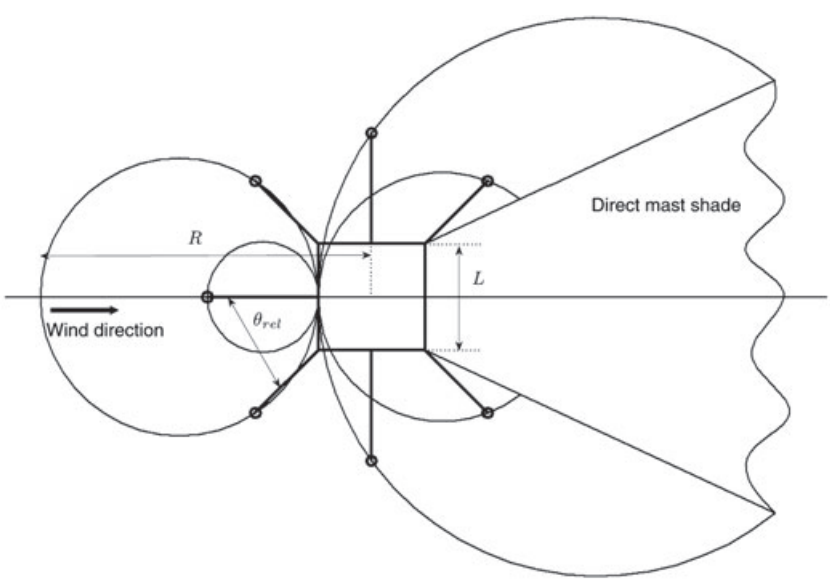

Figure 14. Iso-speed plots of flow around the masts

DOI: 10.1002/we

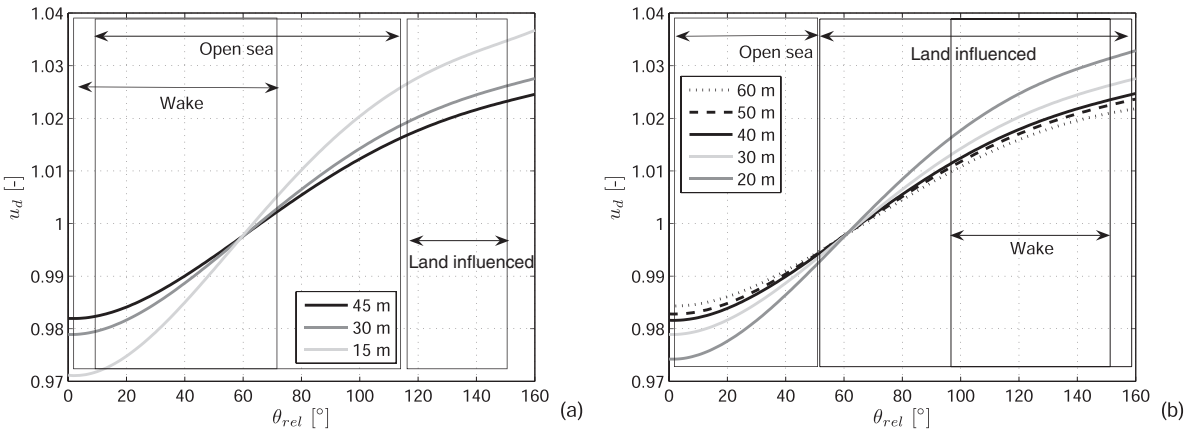

Figure 15. Wind speed deficits for each cup anemometer on all relative wind directions and inflow sectors for (a) M2 and (b) M6

References

1. Stull RB. *An Introduction to Boundary Layer Meteorology*. Kluwer Academic Publishers, 1988.
2. Troen I, Petersen EL. *European Wind Atlas*. Risø National Laboratory, Dordrecht, 1989.
3. Businger JA, Wyngaard JC, Izumi Y, Bradley EF. Flux-profile relationships in the atmospheric surface layer. *Journal of Atmosheric Sciences*, Roskilde, 1971; **28**: 181–189.
4. Gryning S-E, Batchvarova E, Brümmer B, Jørgensen H, Larsen S. On the extension of the wind profile over homogeneous terrain beyond the surface layer. *Boundary-Layer Meteorology* 2007; **124**: 251–268.
5. Lange B, Larsen S, Højstrup J, Barthelmie R. Importance of thermal effects and the sea surface roughness for offshore wind resource assessment. *Journal of Wind Engineering and Industrial Aerodynamics* 2004; **92**: 959–988.
6. Smith DA, Harris M, Coffey AS, Mikkelsen T, Jørgensen HE, Mann J, Danielian R. Wind lidar evaluation at the Danish wind test site in Høvsøre. *Wind Energy* 2006; **9**: 87–93.
7. Mann J, Dellwik E, Bingöl F, Rathmann O. Laser measurements of flow over a forest. Journal of Physics: Conference Series 2007; **75**: 012057.
8. Antoniou I, Jørgensen HE, Mikkelsen T, Frandsen S, Barthelmie R, Perstrup C, Hurtig M. Offshore wind profile measurements from remote sensing instruments. In *Proceedings of the European Wind Energy Association Conference & Exhibition*. Athens, 2006. [Online]. Available: http://www.ewec2006proceedings.info/allfiles2/267_Ewec2006fullpaper.pdf, date accessed 30 June 2008.
9. Kindler D, Oldroyd A, MacAskill A, Finch D. An eight month test campaign of the QinetiQ ZephIR system: preliminary results. *Meteorologische Zeitschrift* 2007; **16**: 479–489.
10. Christiansen MB, Hasager CB. Wake effects of large offshore wind farms identified from satellite SAR. *Remote Sensing of Environment* 2005; **98**: 251–268.
11. Elsam Engineering. Wake effect east of the Horns Rev offshore wind farm. *Technical Report* 209918, Elkraft System, PSO—F&U 2002/FU2103, Eltra no. 4158, ELSAM-VU111, Fredericia, 2005.
12. Pedersen TF. Characterisation and classification of Risø P2546 cup anemometer. *Technical Report* Risoe-R-1364(EN), Risø National Laboratory, Roskilde. 2004. [Online]. Available: http://www.risoe.dk/, date accessed 30 June 2008.
13. 61400-12-1 IEC. *Wind Turbines—Part 12-1: Power Performance Measurements of Electricity Producing Wind Turbines*. International Electrotechnical Commission, Geneva, 2005.
14. Mikkelsen T, Jørgensen HE. Measurement of turbulence with a CW lidar: effects of conical scanning and probe volume. In *Proceedings of the 51st IEA Topical Expert Meeting: State of the Art of Remote Wind Speed Sensing Techniques Using Sodar, Lidar and Satellites*. Roskilde, Thor SE. (ed.), Vattenfall, AB, 2007; 219–233.
15. Burton T, Sharpe D, Jenkins N, Bossanyi E. *Wind Energy Handbook*. John Wiley & Sons Ltd, 2001.
16. Tambke J, Lange M, Focken U, Wolff J-O, John A, Bye T. Forecasting offshore wind speeds above the North Sea. *Wind Energy* 2005; Chichester, **8**: 3–16.
17. Bechmann A. Large-eddy simulation of atmospheric flow over complex terrain. *Technical Report* Risoe-PhD-28(EN), Risø National Laboratory, Roskilde, 2006. [Online]. Available: http://www.risoe.dk/rispubl/reports/ris-phd-28.pdf, date accessed 30 June 2008.

DOI: 10.1002/we

18. Charnock H. Wind stress over a water surface. *Quarterly Journal of the Royal Meteorological Society* 1955; **81**: 639–640.
19. Kraus EB. *Atmosphere-Ocean Interaction*. Oxford University Press, London, 1972.
20. Højstrup J. Vertical extrapolation of offshore wind profiles. In *Proceedings of the European Wind Energy Association Conference & Exhibition*. James & James Science Publishers, Nice, 1999; 1220–1223.

DOI: 10.1002/we